Supplement of Geosci. Model Dev., 15, 8669–8704, 2022
https://doi.org/10.5194/gmd-15-8669-2022-supplement

Geoscientific Model Development Open Access EGU

Supplement of

Implementation and evaluation of the GEOS-Chem chemistry module version 13.1.2 within the Community Earth System Model v2.1

Thibaud M. Fritz et al.

Correspondence to: Sebastian D. Eastham (seastham@mit.edu)

1. Order of routine calls in CAM

CAM performs two sets of calls depending on whether the data has been updated from the land model. The first routine “cam_run1” performs dynamics and atmospheric physics that do not require land model updates, dry adjustment, deep and shallow convection, stratiform macrophysics, MAM wet scavenging and radiation. The second routine "cam_run2" merges the data from the land model and then performs emissions, chemistry, vertical diffusion, Rayleigh friction, MAM dry deposition, gravity wave drag and QBO relaxation.

2. Species mapping between MAM4 and GEOS-Chem species

Table S1 describes the species mapping between MAM4 modal aerosols and GEOS-Chem species.

Table S1: Mapping between MAM4 and GEOS-Chem.

GEOS-Chem species	Mapping to MAM4 species
TSOA0 + ASOAN	soa1_a1 + soa1_a2 + soa2_a1 + soa2_a2
TSOA1 + ASOA1	soa3_a1 + soa3_a2
TSOA2 + ASOA2	soa4_a1 + soa4_a2
TSOA3 + ASOA3	soa5_a1 + soa5_a2
TSOG0	soag0 + soag1
TSOG1 + ASOG1	soag2
TSOG2 + ASOG2	soag3
TSOG3 + ASOG3	soag4
SO4	so4_a1 + so4_a2 + so4_a3 + H2SO4
BCPI	bc_a1
BCPO	bc_a4
OCPI	pom_a1
OCPO	pom_a4
DST1	dst_a1 + dst_a2
DST2	None
DST3	None
DST4	dst_a3

SALA	ncl_a1 + ncl_a2
SALC	ncl_a3

3. Mapping between CLM biogenic emission species and GEOS-Chem species

Table S2 presents the mapping between GEOS-Chem species and MEGAN biogenic emission species as calculated in CLM. Mapping to CAM-chem species is listed in the Supplementary Information of Emmons et al. (2020).

Table S2: Mapping between GEOS-Chem species and MEGAN species in CLM

GEOS-Chem species	MEGAN species in CLM
ISOP	isoprene
MOH	methanol
EOH	ethanol
CH2O	formaldehyde
ALD2	acetaldehyde
ACTA	acetic_acid
ACET	acetone
HCOOH	formic_acid
None	hydrogen_cyanide
CO	carbon_monoxide
C2H6	ethane
C2H4	ethene
C3H8	propane
ALK4	pentane + hexane + heptane + tricyclene
PRPE	propene + butene
TOLU	Toluene
LIMO	Limonene
MTPA	pinene_a + pinene_b + sabinene + carene_3
MTPO	terpinene_g + terpinene_a + terpinolene + myrcene + ocimene_al + ocimene_t_b + ocimene_c_b + thujene_a + 2met_styrene + cymene_p + cymene_o + bornene + fenchene_a + camphene + phellandrene_a + phellandrene_b

4. Emissions mapping in C-GC, C-CC, and S-GC

Table S3 presents the emissions mapping between HEMCO and all three models considered in this study.

Table S3: Emissions mapping from HEMCO to C-GC, C-CC, and S-GC

Emission species	C-GC	C-CC	S-GC
MOH	MOH	CH3OH	MOH
EOH	EOH	C2H5OH	EOH
ROH	ROH	-	ROH
C2H6	C2H6	C2H6	C2H6
C3H8	C3H8	C3H8	C3H8
C4H10	ALK4	BIGALK	ALK4
C5H12	ALK4	BIGALK	ALK4
C6H14	ALK4	BIGALK	ALK4
C2H4	C2H4	C2H4	C2H4
PRPE	PRPE	C3H6	PRPE
C2H2	C2H2	C2H2	C2H2
BENZ	BENZ	BENZENE	BENZ
TOLU	TOLU	TOLUENE	TOLU
XYLE	XYLE	XYLENES	XYLE
TMB	-	XYLENES	-
OTAR	-	XYLENES	-
CH2O	CH2O	CH2O	CH2O
ALD2	ALD2	CH3CHO	ALD2
MEK	MEK	MEK	MEK
ACE	-	CH3COCH3	-
HCOOH	HCOOH	HCOOH	HCOOH
C2OH	-	CH3COOH	-
EOH	EOH	C2H5OH	EOH
MACR	MACR	MACR	MACR
ACET	ACET	CH3COCH3	ACET
BCPI	bc_a*	bc_a*	BCPI
OCPI	pom_a*	pom_a*	OCPI
SO4	so4_a1/so4_a2	so4_a1/so4_a2	SO4

5. Dust emissions in CESM

Emissions of dust in CESM are calculated through the Community Land Model (CLM), with a resolution-dependent scaling factor applied. For this work, we use the same scaling factor (0.24) for both C-CC and C-GC, resulting in dust emissions of 5,894 Tg per year. This is significantly greater than the ~3,000 Tg/yr reported by Emmons et al. (2020), due to the use of a different scaling factor and resolution in that work.

As discussed by Tilmes et al. (2016), the dust emissions scaling factor in CESM is typically tuned to achieve an annual mean dust aerosol optical depth (AOD) of 0.025 – 0.030. We find AODs of 0.04 in C-GC, and 0.08 in C-CC. This suggests that dust removal in C-GC is roughly twice as efficient as in C-CC. This implies that the scaling factor should be reduced in future usage of C-GC or C-CC. The combination of C-GC's relatively small overestimate in dust AOD and the large total dust emissions also implies that dust scavenging in C-GC may be too rapid.

6. Scavenging scheme

Figure S1 shows the calculated wet removal rate of HNO_3 in all three models. Positive values correspond to rain re-evaporation at low altitudes re-releasing dissolved HNO_3. The Neu scavenging scheme in C-GC and C-CC results in an HNO_3 wet removal rate which is four times higher in C-GC than in S-GC. This likely explains the greater depletion of HNO_3 in the mid-troposphere calculated by C-GC compared to S-GC, as shown in Figure 11. Wet scavenging in C-CC is faster yet, with HNO_3 wet removal rates approximately six times greater than in S-GC, and 50% greater than in C-GC. This is in part because the mixing ratio (or fraction of total NO_y) of HNO_3 in the mid- and upper-troposphere as modeled in C-CC is greater than in either C-GC or S-GC, but also because C-GC and S-GC simulate nitrate aerosol explicitly.

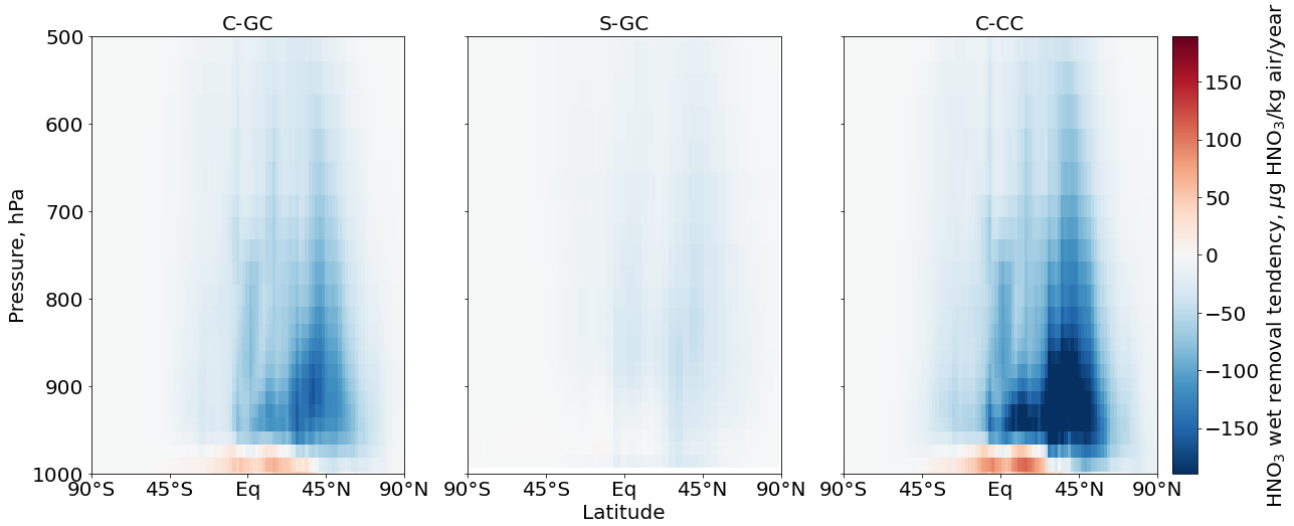

Figure S1: Annual zonal mean of nitric acid wet removal tendencies for C-GC (left), S-GC (middle), and C-CC (right).

The application of the Neu scheme to remove nitrate aerosol also affects removal of total NO_y in C-GC. Figure S2 shows the annual mean wet removal rates of the nitrate aerosol tracer NIT in C-GC and S-GC. The Neu scheme removes aerosol more rapidly than the scheme used in S-GC, and at lower altitudes.

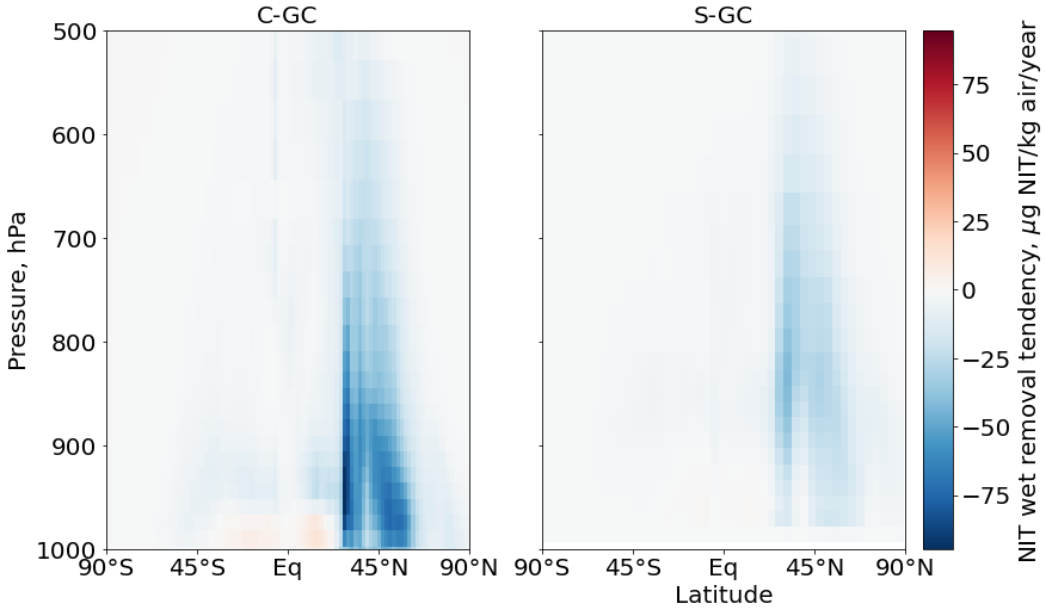

Figure S2: Annual zonal mean of nitrate aerosol (NIT) wet removal tendencies for C-GC (left) and S-GC (right). Nitrate aerosols are not modeled in CAM-chem.

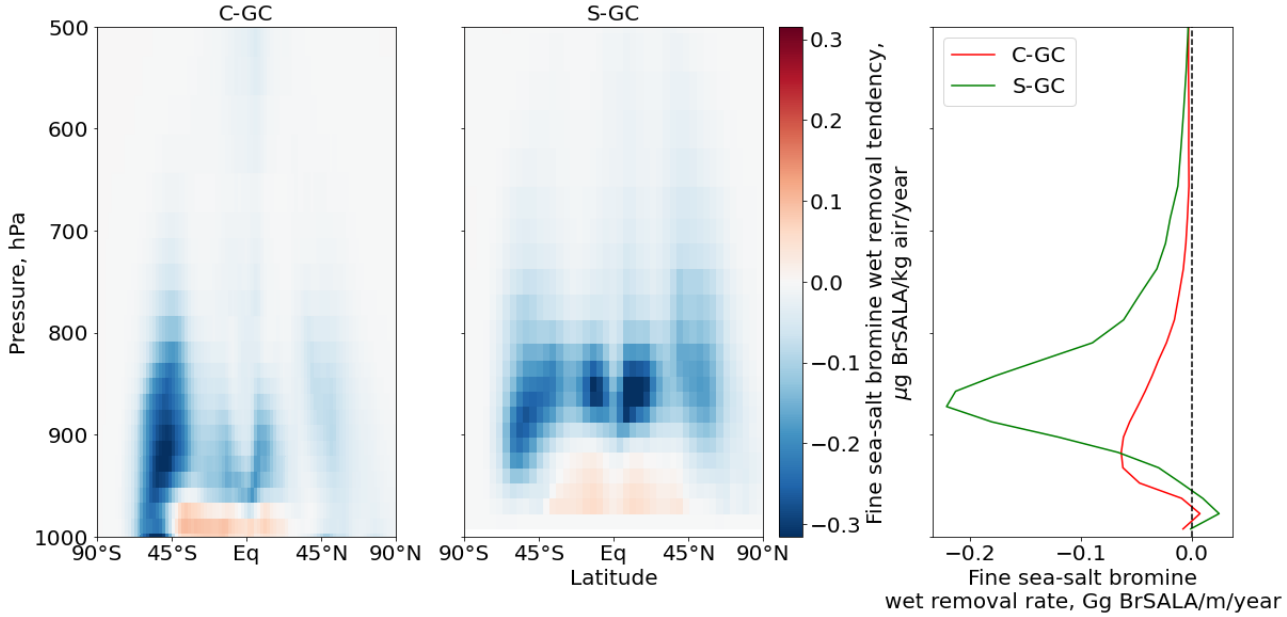

Figure S3. Zonal mean wet removal tendency of bromine carried in fine sea salt**.** Left and middle: Removal rates calculated by C-GC (left) and S-GC (middle). Right: Annual mean of fine sea salt bromine aerosol wet removal rate for C-GC (red), S-GC (green). Bromine in sea-salt aerosol is not modeled in CAM-chem.

7. Surface-level NO_2, NO_x and $NO:NO_2$ ratio

Figure S4 shows the global distribution of NO_2 and of NO_x ($NO + NO_2$). These data are provided to supplement Figure 17 in the main text, and thus provides some insight into possible causes of disagreements.

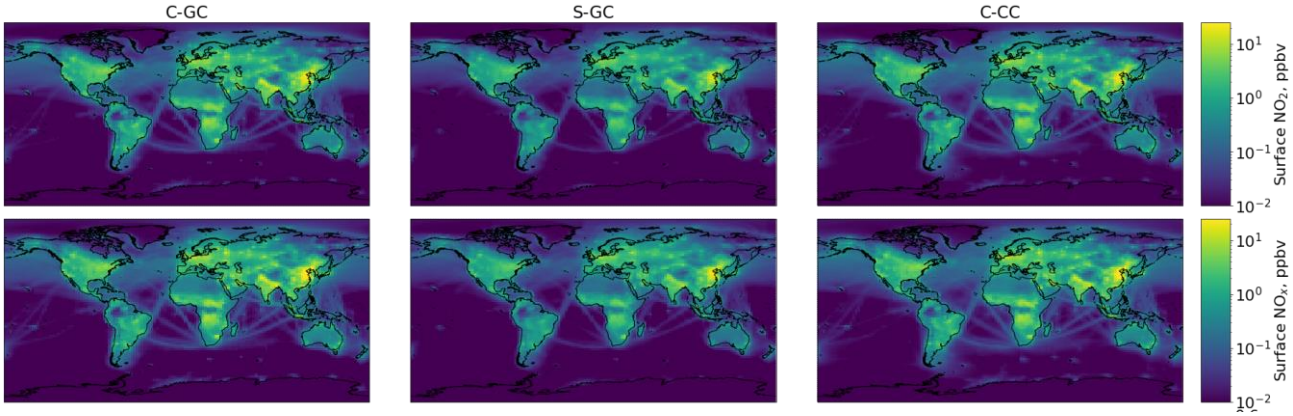

Figure S4: Surface-level NO_2, NO_x, and $NO:NO_2$ estimated by C-GC (left), S-GC (middle), and C-CC (right) for 2016. Top: annual average NO_2 in ppbv. Bottom: annual average NO_x ($NO + NO_2$) in ppbv..

8. Representations of in-cloud sulfur oxidation in the GEOS-Chem chemistry modules and MAM

Two representations of in-cloud sulfur oxidation exist in C-GC: from the GEOS-Chem chemistry modules and in MAM. For C-GC, we choose to use the GEOS-Chem representation of in-cloud sulfur oxidation, such that the GEOS-Chem chemistry module remains identical to that of the GEOS-Chem CTM. However, this makes C-GC and C-CC, both embedded in CESM2, rely on different processes to perform sulfur oxidation in clouds. The routines responsible for in-cloud sulfur oxidation in MAM are bypassed when running C-GC.

Previous versions of C-GC double counted in-cloud sulfur oxidation. We here perform two test runs of C-GC for January 2015 before and after the sulfur oxidation bugfix - which introduces the bypass of the routines in MAM responsible for in-cloud sulfur oxidation. Figures S5 and S6 display the relative difference in zonal SO_2 and SO_4 attributable to the MAM in-cloud sulfur routines. Implementing this bugfix increases SO_2 and decreases SO_4, enhancing the SO_2 burden by ~5 to 10%.

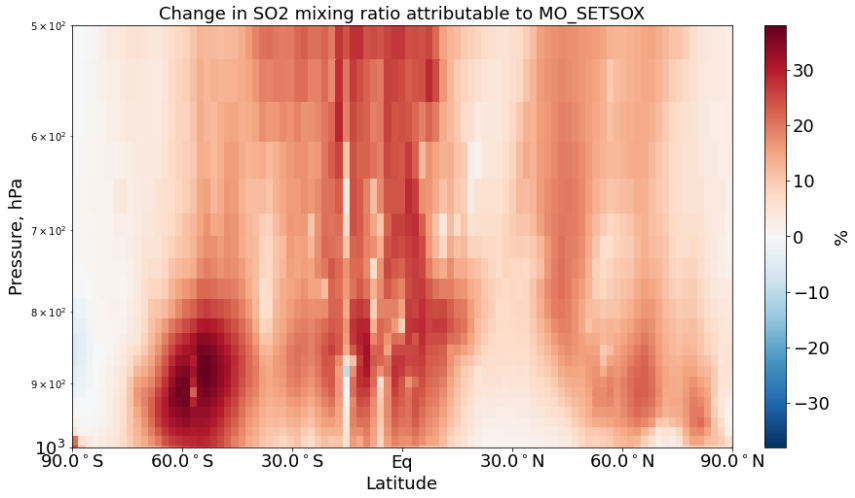

Figure S5: Relative difference in zonally-averaged sulfur dioxide mixing ratios up to 500 hPa due to in-could sulfur oxidation as evaluated by MAM.

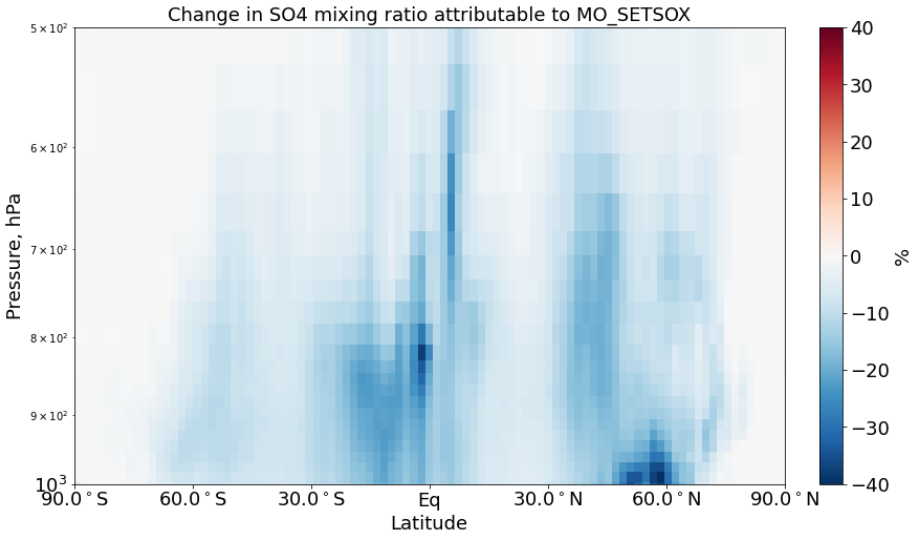

Figure S6: Relative difference in zonally-averaged sulfate aerosols mixing ratios up to 500 hPa due to in-could sulfur oxidation as evaluated by MAM.

9. Non-linear chemistry during the Antarctic spring

This section focuses on the changes in atmospheric composition above the South Pole for C-GC and S-GC. Figures S7, S8, and S9 respectively display active chlorine, inactive chlorine, and ozone, averaged over the 80°S - 90°S latitude band for C-GC and S-GC for 2015 and 2016.

For both C-GC and S-GC, we observe strong production of active chlorine during austral winter. The peak active chlorine mixing ratio is greater in S-GC by ~15%. Correspondingly, we find that reservoir species of chlorine are depleted during austral winter in the 10 to 100 hPa altitude band in both models.

In both models, we find that ozone is depleted during the Antarctic spring (from September to December) due to the presence of active halogens and sunlight. We find that the magnitude of the ozone hole matches from one year to the other in both models (2015 appears to have a more significant ozone hole than 2016). We also find that during the Antarctic spring, ozone around 10 hPa increases in both C-GC and S-GC.

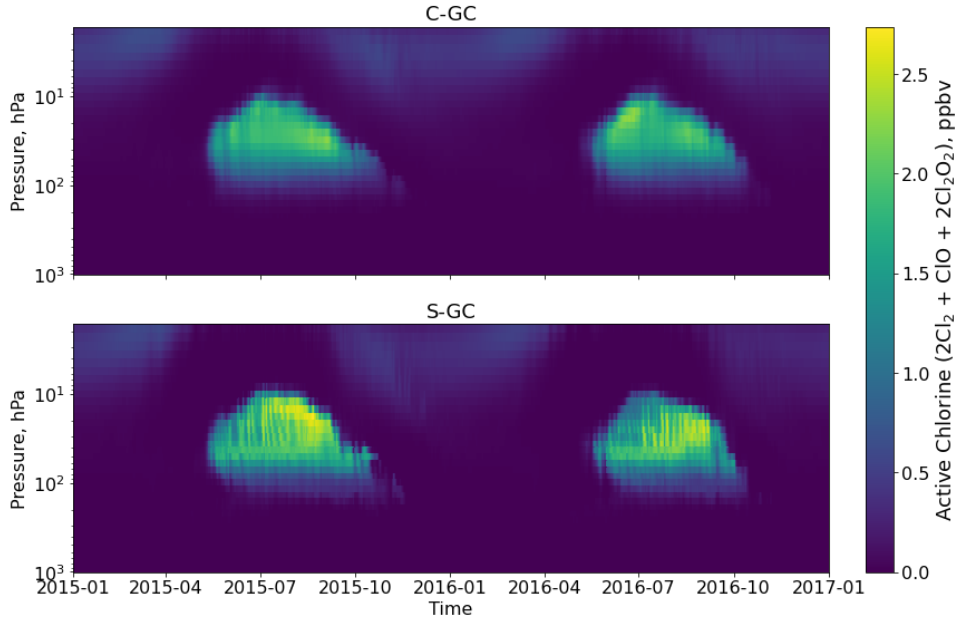

Figure S7: Temporal evolution of active chlorine averaged over the 80°S - 90°S latitude band for C-GC (top) and S-GC (bottom).

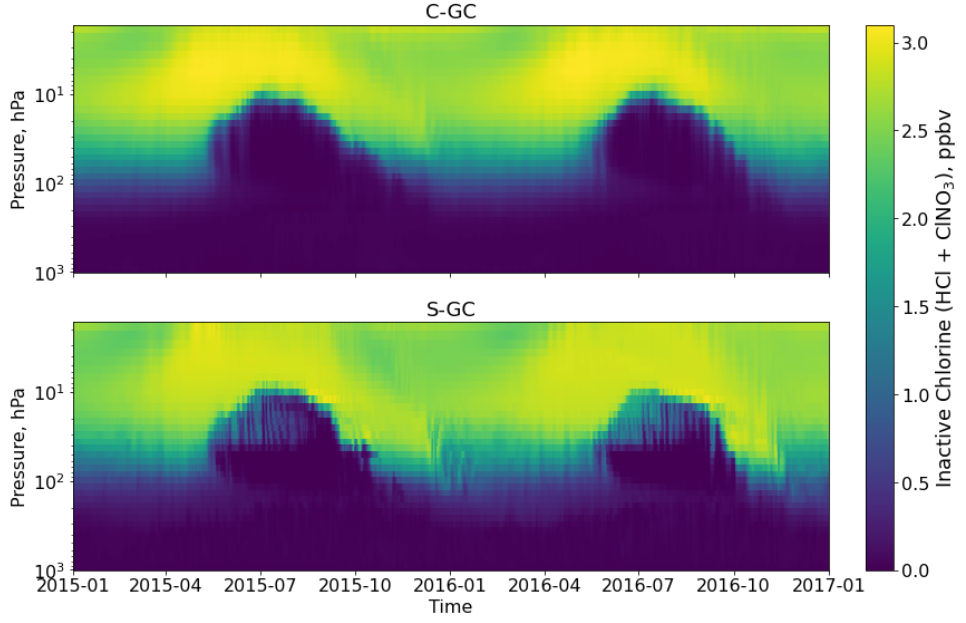

Figure S8: Temporal evolution of inactive chlorine averaged over the 80°S - 90°S latitude band for C-GC (top) and S-GC (bottom).

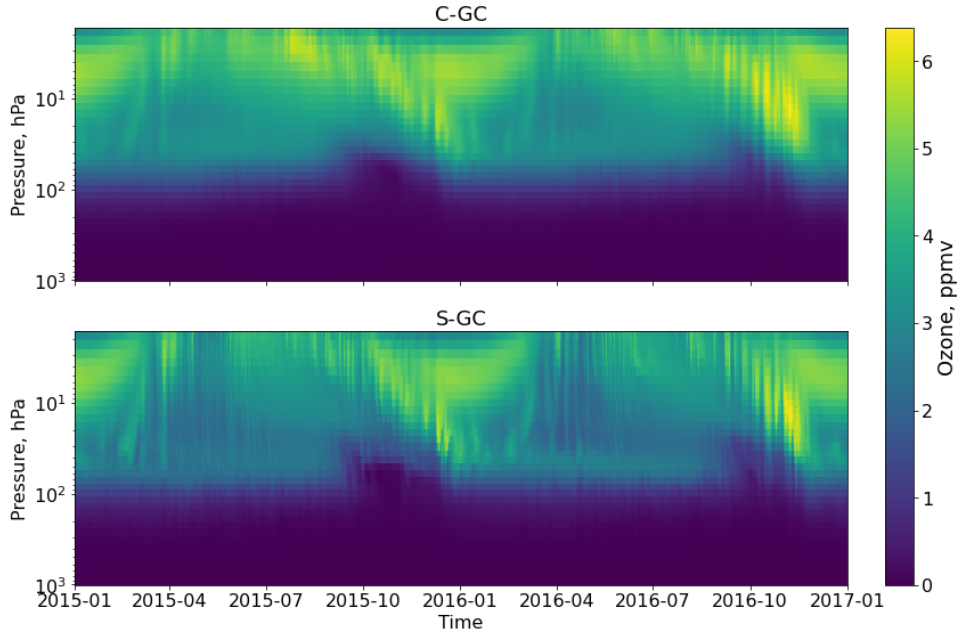

Figure S9. Temporal evolution of ozone averaged over the 80°S - 90°S latitude band for C-GC (top) and S-GC (bottom).

Figure S10 displays the minimum ozone column in the 80°S - 90°S latitude band from C-GC and S-GC against measurements from the NASA Ozone Watch (https://ozonewatch.gsfc.nasa.gov/, last accessed 7 January 2022).

During the Antarctic spring, we find that C-GC more accurately reproduces the dip in the ozone column, but this could be due to differences in the horizontal resolution. We also find that both models fail to capture the increase in the South Pole ozone column between May and July for both 2015 and 2016.

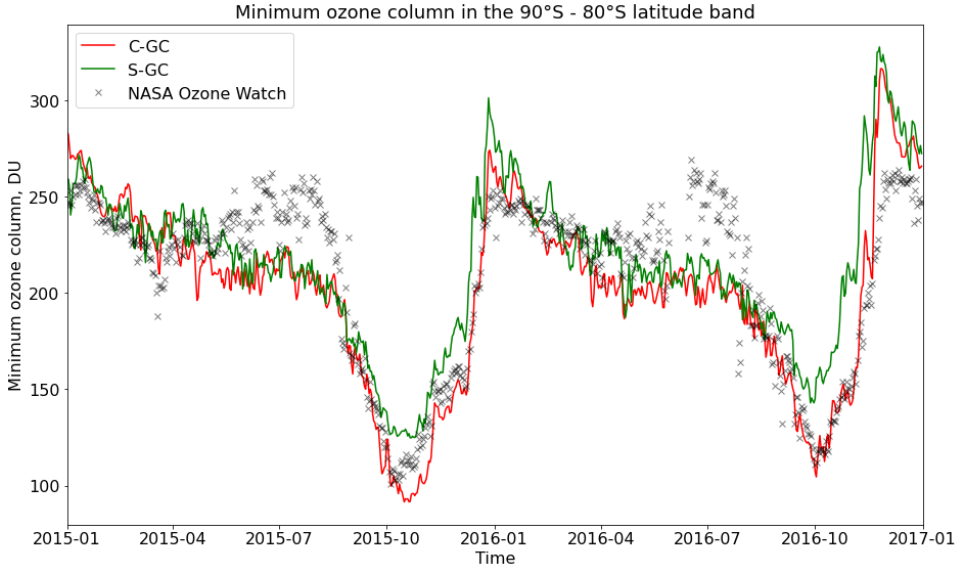

Figure S10: Temporal evolution of minimum ozone column averaged over the 80°S - 90°S latitude band for C-GC (blue) and the GEOS-Chem CTM (red).